ISSN: 2472-3703 DOI: 10.6911/WSRJ.202106_7(6).0010

Research on Unloading Mechanism of Red Sandstone Based on Ansys

Haixiao Lin[1], Xu Zhang[1, a, *], Tao Wang[2], Long Cheng[1]

[1]School of Civil Engineering, Henan Polytechnic University, Jiaozuo, China

[2]CSCEC Zhongyuan Architectural Design Institute Co.Ltd, Zhengzhou, China

[a]1205466762@qq.com

Abstract

Based on the software development function of Ansys, a parametric programming language is written to study the unloading mechanism of rock samples. Comparing the change characteristics of strain energy density in the loading test, the strain energy density in the unloading test is released along both sides as the minimum principal stress gradually decreases. The failure mode is tensile-shear coupling failure, which may be due to the tensile stress generated by unloading resulting in. And as the lateral stress gradually decreases, the minimum bearing area gradually increases.

Keywords

Red sandstone; Prefabricated cracks; Ansys; Unloading mechanism.

1. INTRODUCTION

In response to the call for maximum utilization of resources, more and more underground projects have been put into construction, and the problem of project construction safety comes with it. Natural rock masses usually contain various joints and tectonic surfaces and are in a state of stress balance. However, due to the natural environment and man-made disturbances, the rock mass will lose balance and redistribute stress, which will lead to engineering disasters. Therefore, it is of great significance to carry out research on the mechanism of rock loading and unloading. Li et al. [1] used a series of conventional triaxial and true triaxial tests, combined with acoustic emission to study the deformation characteristics of rock samples and the influence of intermediate principal stress. Du et al. [2] conducted true triaxial compression tests on three types of rocks, and studied the effects of different intermediate principal stresses and minimum principal stresses on the failure characteristics. He et al. [3] defined deep rock masses, that is, as the excavation depth increases, the underground engineering rock masses appear nonlinear mechanical phenomena. Non-linear mechanical phenomena refer to large deformations of soft rocks or rock bursts (rockbursts) of hard rocks. The excavation of underground engineering is accompanied by radial unloading, that is, the initial three-dimensional stress state changes to a biaxial or uniaxial stress state. At this time, due to the effect of unloading stress, stress adjustment occurs inside the sample. In order to study the change of stress state during excavation of working face in underground engineering, Yin et al. [4] simulated the excavation rate of underground engineering by designing different stress unloading rate tests to study the relationship between unloading rate and mechanical properties of rock mass, and found that the rate of unloading varies with the unloading rate. Increasing the capacity of the rock mass becomes more obvious and the capacity expansion increases, while the proportion of dissipated energy at the time of failure gradually decreases. Xu et al. [5] concluded that instantaneous failure is easy to occur at high unloading rates, but progressive failure is not easy to occur. In this paper, the mechanism of loading and unloading failure is studied through a combination of physical experiment and numerical simulation.

ISSN: 2472-3703 DOI: 10.6911/WSRJ.202106_7(6).0010

2. EXPERIMENT DESIGN AND EXPERIMENT MECHANISM

2.1. Sample Design

The test uses red sandstone without obvious joints, cuts it into a rectangular parallelepiped with a size of 50mm×50mm×100mm, and carefully grinds it until the non-parallelism and non-perpendicularity are both less than 0.02mm. Then use the method of drilling holes and then cutting the joints to prefabricate the cracks. The joint length 2a is 20mm, the joint width is 1mm, and the prefabricated crack inclination angle α is 45°, as shown in Figure 1. The basic physical and mechanical parameters of red sandstone measured by the RMT150-B rock mechanics testing machine are shown in Table 1.

Figure 1. Prefabricated cracked red sandstone

Table 1. Basic physical and mechanical parameters of red sandstone

Natural density ρ (g/cm3)	Peak intensity (MPa)	Poisson's ratio ν	Elastic Modulus E(GPa)	Tensile strength (MPa)
2.39	117	0.243	27.4	3.8

2.2. Test Equipment and Test Plan

The test instrument uses the GCTS RTX-3000 high temperature and high pressure rock triaxial test machine, as shown in Figure 2. The test system consists of a main controller, a loading frame, a confining pore pressure booster controller, a rapid pulse attenuation test device, and a hydraulic pump station. It consists of five parts. The maximum axial pressure of the testing machine is 3000kN, the maximum stroke is 100mm, the maximum confining pressure is 140MPa, and the maximum pore pressure is 140MPa. During the test, the lateral and axial displacement sensors are installed on the sensor frame respectively, and the LVDT is used to measure the axial and lateral deformation with a range of 2.5mm. At the same time, in order to increase the stroke of the hydraulic sheet in the true triaxial pressure chamber, the test is usually performed Add four shims around the sample.

The loading test plan is as follows. First, load the three principal stress directions to the hydrostatic pressure state (σ1=σ2=σ3) at a stress loading rate of 0.1MPa/s, and then keep σ3 unchanged, and load σ1 and σ2 to the same stress loading rate. The predetermined value of σ2, and finally the values of σ2 and σ3 are kept unchanged, and converted into displacement controlled loading, which is loaded at 0.001mm/s until the specimen is broken. As shown in Figure 3.

ISSN: 2472-3703 DOI: 10.6911/WSRJ.202106_7(6).0010

The unloading test plan is as follows. First, load the three principal stress directions to the hydrostatic state (σ1=σ2=σ3) at a stress loading rate of 0.1MPa/s, and then keep σ3 unchanged, and load σ1 and σ2 at the same stress loading rate. To the predetermined value of σ2, finally keep the values of σ2 and σ3 unchanged, and convert to displacement controlled loading. The loading is stopped when it is loaded to 60% of the true triaxial strength of the specimen at 0.001mm/s, and then σ1 and σ2 remain unchanged to Unload σ3 to 0 at 0.1MPa/s, and finally continue to load σ1 at 0.1MPa/s until the rock fails, as shown in Figure 4.

Figure 2. GCTS RTX-3000 rock mechanics system

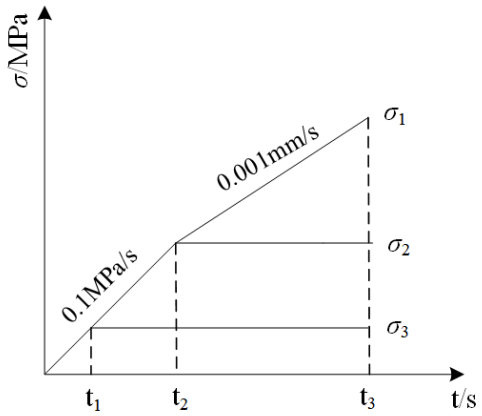

Figure 3. Schematic diagram of loading path

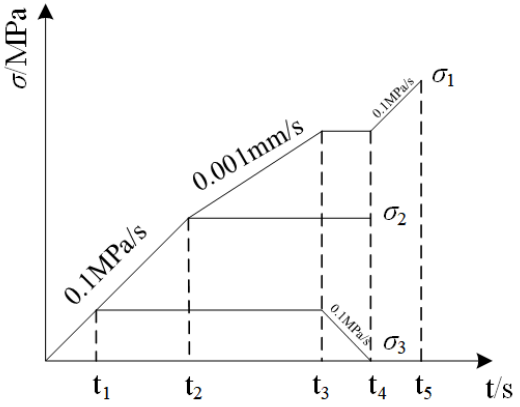

Figure 4. Schematic diagram of unloading path

3. COMPARATIVE ANALYSIS OF LOADING AND UNLOADING TESTS

In the experiment, design σ_3=5MPa, σ_2=30MPa, and then load according to the loading test plan in Section 2-2. The measured stress-strain curve is shown in Figure 5(a). The true triaxial compressive strength under this stress state is 151.2 MPa. According to the true triaxial compression strength, the initial stress state in the unloading test is determined. Therefore, when the maximum principal stress is loaded to 100MPa, the minimum principal stress will be unloaded. The stress-strain curve is shown in Figure 5(b). The comparison of the two figures shows that the stress-strain curve changes in the three directions before unloading are similar. The minimum principal stress direction curve changes gradually when the load is close to failure. The maximum principal stress direction curve rises rapidly and then suddenly drops. The stress, the minimum principal stress direction curve changes very much, and the sample will be damaged after a long time of stress redistribution.

ISSN: 2472-3703 DOI: 10.6911/WSRJ.202106_7(6).0010

Figure 6 is the failure diagram of the loaded and unloaded sample. It can be seen from the figure that the loading failure of the prefabricated red sandstone with 45° cracks is the shear failure caused by the penetration of the anti-wing crack, and the failure mode is relatively complete. From Figure 6 (b) It can be seen that the unloading failure does not penetrate the upper and lower ends of the sample along the anti-wing cracks on both sides, the left side produces tensile failure along the unloading direction, and the right side produces shear failure.

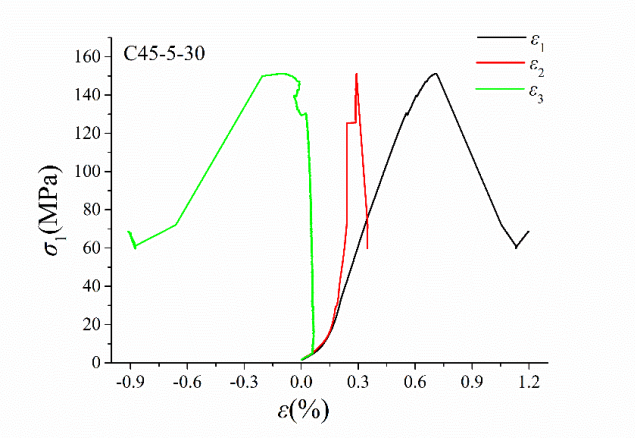

(a) Red sandstone loading stress-strain curve

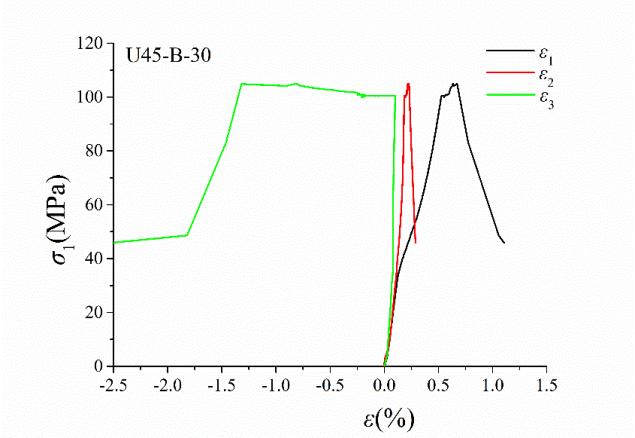

(b) Red sandstone unloading stress-strain curve

Figure 5. Load-unload stress-strain curve of red sandstone with 45° prefabricated cracks

(a) Red sandstone loading failure mode diagram (b) Unloading failure mode diagram of red sandstone

Figure 6. Loading and unloading failure mode diagram of red sandstone with 45° prefabricated cracks

ISSN: 2472-3703 DOI: 10.6911/WSRJ.202106_7(6).0010

4. NUMERICAL SIMULATION

4.1. Damage Evolution Constitutive Relationship

According to the Lemaitre strain equivalence principle [6], the strain produced by effective stress acting on the non-destructive material is equal to the strain produced by the stress acting on the lossy material. Based on this, the basic relationship of rock damage constitutive is established [7]:

$$[\sigma]=[\sigma^*](1-D)=[c][\varepsilon](1-D)$$

In the above formula: [σ] is the material stress matrix, [σ*] is the effective stress matrix, [c] is the material elastic matrix, [ε] is the material strain matrix, and D is the damage variable.

Based on the elastic constitutive relations of uniaxial tension and uniaxial compression, the elastic damage constitutive relations of meso-elements under uniaxial stress are given. When the meso-element reaches the maximum tensile strain or the threshold of the Mohr-Coulomb criterion, the meso-element is damaged [8]. According to rock mechanics regulations, compressive stress or compressive strain is always positive, and tensile stress or tensile strain is always negative. Figure 7 shows the elastic damage constitutive relationship used in this article. The expression of damage variable under uniaxial tension is:

$$D=\begin{cases}0 & \varepsilon_{t0}\le\varepsilon<0\\ 1-\dfrac{\sigma_{tr}}{E_0\varepsilon} & \varepsilon_{tu}\le\varepsilon<\varepsilon_{t0}\\ 1 & \varepsilon\le\varepsilon_{tu}\end{cases}$$

σ_{tr} is the residual strength of the mesoscopic element, ε_{t0} is the tensile damage strain threshold, ε_{tu} is the ultimate tensile strain of the element, and E_0 is the initial elastic modulus.

Similarly, the damage variable expression under uniaxial compression is:

$$D=\begin{cases}0 & \varepsilon<\varepsilon_{c0}\\ 1-\dfrac{\sigma_{cr}}{E_0\varepsilon} & \varepsilon\ge\varepsilon_{c0}\end{cases}$$

σ_{cr} is the residual strength of the meso-elements, and ε_{c0} is the maximum compressive principal strain corresponding to the uniaxial compressive strength.

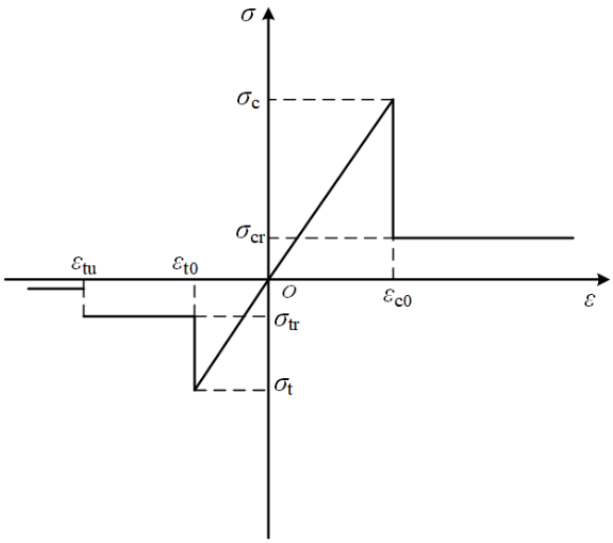

Figure 7. Elastic damage constitutive relation of mesoscopic element

ISSN: 2472-3703 DOI: 10.6911/WSRJ.202106_7(6).0010

4.2. Ansys Software Development

This article uses Ansys Parametric Design Language (APDL) as a scripting language for modeling and analysis operations. APDL's programming language can be used to change parameters and function loops to perform repeated operations to improve efficiency; or to write some through APDL The frequently used programs are then saved as macro files for subsequent recall.

Figure 8 is a simplified diagram of the APDL programming language and calculation area written during modeling. The model is a plane model, the size of the model is the same as the real sample, the lower end of the model is constrained in 3 directions, and the other surfaces are free. Figure 9 shows the loading and unloading programming language, through debugging and analyzing the number of steps, load size and loading rate to achieve the best calculation results.

```
/Prep7
W=50
H=100
wprota,-45,0,0
blc4,-0.5,-10,1,20
wpoffs,,-10
cyl4,0,0,0,0,0.5,-180
wpoffs,,10
wpoffs,,10
cyl4,0,0,0,0,0.5,180
wpoffs,,-10
wprota,45,0,0
nummrg,all
numcmp,all
aadd,1,2,3
blc4,-25,-50,W,H
asba,1,4
nummrg,all
numcmp,all
allsel,all
ET,1,PLANE182
```

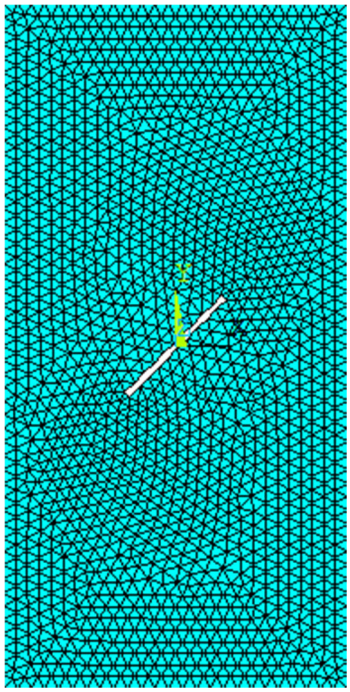

Figure 8. (a) Modeling programming language (b) A schematic diagram of the calculation area

```
SN=30
sbn=100
DIS=0.04
incDIS=0.4E-2
!!!!!!!!!!!!
CF=0
incCF=0!2e6
LCF=20e6
```

```
SN=40
sbn=100
DIS=0.04
incDIS=0.4E-2
!!!!!!!!!!!!
TCF=40e6
incLCF=-0.5e6
LCF=20e6
```

Figure 9. (a) Loading language (b) Unloading language

4.3. Load Failure Strain Energy Density Diagram

In order to observe the failure process of the sample loaded, Figure 10 shows the strain energy density diagram of using Ansys to simulate the loading failure process of the sample with prefabricated cracks.

ISSN: 2472-3703 DOI: 10.6911/WSRJ.202106_7(6).0010

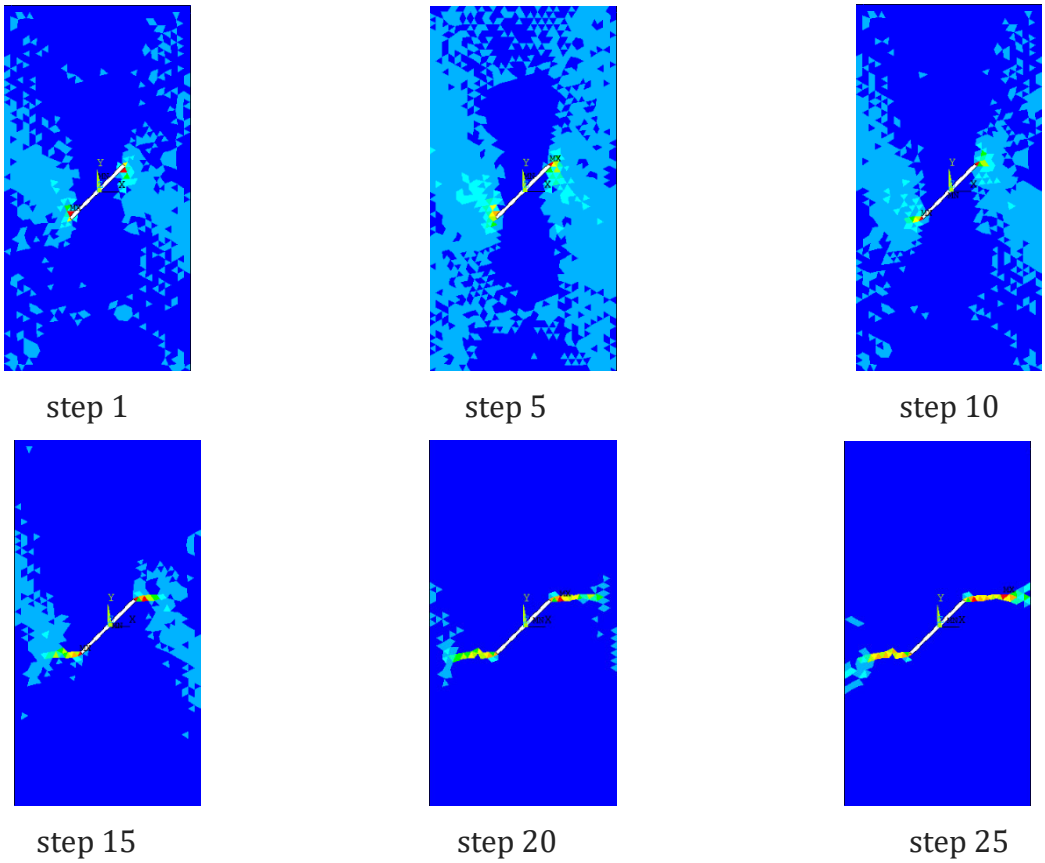

Figure 10. Strain energy density diagram during loading

It can be seen from the figure that step1~step10 are the strain energy density diagrams at the initial stage of loading. It is found that the strain energy density at the crack tip is the largest. The strain energy density on both sides of the sample gradually decreases as the distance from the two ends of the crack is farther, and the overall strain energy The density distribution is in an "X" shape. With further application of load, in step15, the larger strain energy density is mainly concentrated near the prefabricated crack, and the strain energy density at the crack tip is also the largest. In the final load phase, step 25, the specimen forms a release path with a greater strain energy density. The final release path of strain energy shows that the failure mode produced by loading is relatively complete.

4.4. Unloading Failure Strain Energy Density Diagram

Figure 11 is a graph of strain energy density of different calculation steps for simulating the unloading test of a sample containing prefabricated cracks. In step 1, the initial unloading stage, the maximum strain energy density is at the crack tip, followed by the two sides of the sample, and the smallest strain energy density in the middle of the sample. With the continuous decrease of the stress on both sides of the specimen, the strain energy density near the unloading end continues to increase, and the minimum strain energy density area continues to increase. According to step 30, it can be found that the unloading damage is relatively broken, especially on both sides of the unloading. The analysis may be caused by the tensile stress generated by the unloading.

In order to further analyze the change of strain energy density inside the sample during the unloading process, the APDL programming language was written to select the minimum strain energy density region during different unloading stages, as shown in Figure 12.

ISSN: 2472-3703 DOI: 10.6911/WSRJ.202106_7(6).0010

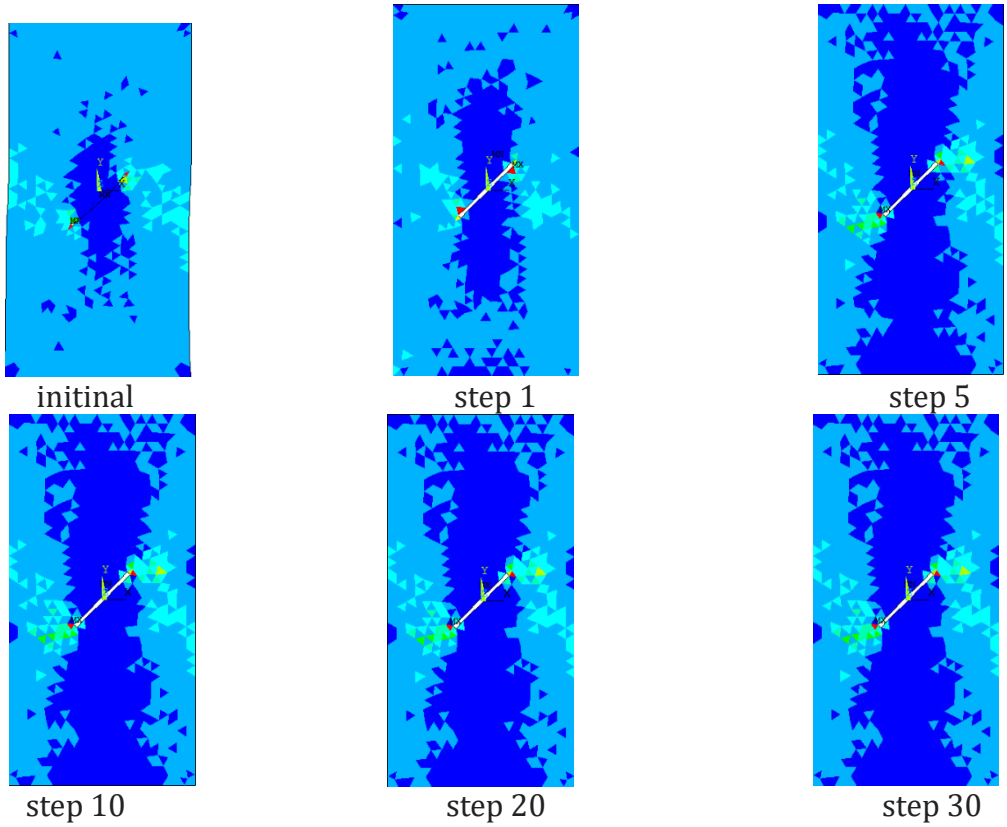

Figure 11. Strain energy density diagram in unloading process

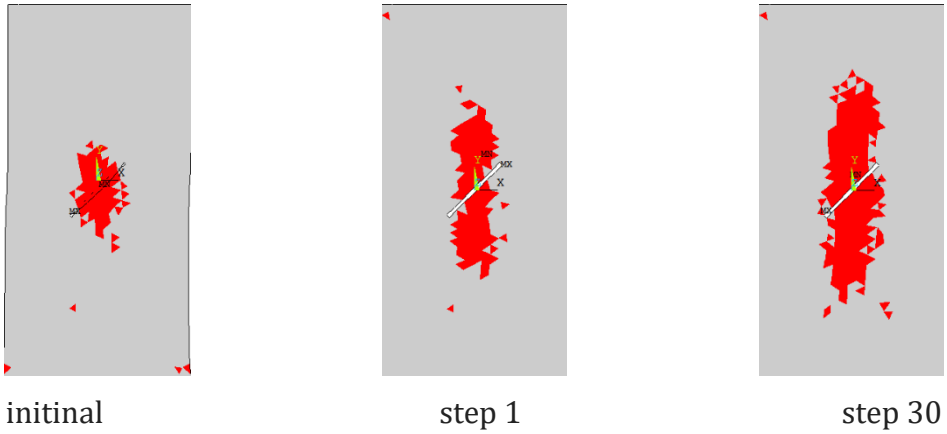

Figure 12. Minimum strain energy density diagram in unloading process

The red area in Figure 12 is the minimum strain energy density area. It can be seen from the figure that the minimum load-bearing area (red area) increases as the stress on both sides continues to decrease, indicating that the strain energy is continuously released during the unloading process, and the specimen is loaded The force gradually decreases.

5. CONCLUSION

Based on Ansys numerical simulation, this paper studies the unloading mechanism of sandstone specimens from two aspects of strain energy density and minimum bearing area, and draws the following conclusions:

(1) The strain energy density distribution inside the specimen during loading failure is different from that during unloading failure. In the loading test, the strain energy accumulates continuously at the initial stage, and it is suddenly released along the path of maximum strain

ISSN: 2472-3703 DOI: 10.6911/WSRJ.202106_7(6).0010

energy when it is close to failure. In the unloading test, the strain energy is It is continuously released during the unloading process, and its damage gradually accumulates as the minimum strain energy density area increases until it fails.

(2) In the unloading test, the minimum load-bearing area gradually increases with the decrease of the minimum principal stress until the sample completely loses the load-bearing capacity and damage occurs.

(3) The loading failure mode is relatively complete as a whole, and it is only released along the region with higher strain energy density. During unloading failure, the internal damage will gradually accumulate with the continuous decrease of the minimum principal stress, so the failure mode is relatively fragmented.

REFERENCES

[1] Z.L. Li, L.G. Wang, Y.L. Lu, et al. Experimental investigation on True Triaxial Deformation and Progressive Damage Behaviour of Sandstone. Scientific Reports, Vol. 9 (2019) No. 1, p.3386.

[2] K. DU, C.Z. Yang, R. Su, et al. Failure properties of cubic granite, marble, and sandstone specimens under true triaxial stress[J]. International Journal of Rock Mechanics and Mining Sciences, Vol. 130 (2020) , p.104309.

[3] M.C. He, J.L. Miao, D.J. Li, et al. Experimental Study on Rockburst Process of Deep Granite Sample. Chinese Journal of Rock Mechanics and Engineering, Vol. 26 (2007) No. 005, p.865-876.

[4] G.Z. Yin, B. Ma, C. Liu, et al. Effects of loading and unloading rates on the mechanical properties and energy characteristics of sandstone under true triaxial stress conditions. Journal of China Coal Society, Vol. 44 (2019) No. 2, p.454-462.

[5] H. Xu, X.T. Feng, C.X. Yang, et al. Influence of initial stresses and unloading rates on the deformation and failure mechanism of Jinping marble under true triaxial compression. International Journal of Rock Mechanics and Mining Sciences, Vol. 117 (2019) , p.90-104.

[6] LEMAITRE J. How to use damage mechanics. Nuclear Engineering and Design, Vol. 80 (1984) No. 2, p.233-245.

[7] W.G. Cao, M.H. Zhao X.J. Tang. A study on damage statistical strength theory for rock. Chinese Journal of Geotechnical Engineering, Vol.26 (2004) No.64, p.184-187.

[8] W.C. Zhu, C.A. Tang, Y.H. Yang, et al. The constitutive relationship and verification of meso-unit of the (RFPA~(2D)) system for rock failure process analysis. Chinese Journal of Rock Mechanics and Engineering, Vol.22 (2003) No.1, p.24-29.